ISSN 1392–1320 MATERIALS SCIENCE (MEDŽIAGOTYRA). Vol. XX, No. X. 2021

Shape Memory Alloy Hybrid Composites for Improving Impact Properties

Chuanliang SHEN, Xiaodong XU, Xiaoyu MA, Yibo HU, Shan ZHANG, Yingchen DU, Zhenhai GAO *

State Key Laboratory of Automotive Simulation and Control, Jilin University, 5988 Renmin Street, Changchun 130025, China

crossref http://dx.doi.org/10.5755/j02.ms.24503

Received 04 November 2019; accepted 11 February 2020

This paper investigates the method to improve the property that can decrease the impact response of composite plate. Embedding the super-elastic shape memory alloy wires into composite plates has increased the attention of material researchers. Super-elastic shape memory alloy has the properties of absorbing mechanical energy, large recoverable deformation and so on. In this study, experiments were conducted to analyze the impact properties of composite plates with Ni-Ti SMA wires. Composite plates with Ni-Ti SMA wires and without Ni-Ti SMA wires were subjected to two impacts respectively. This study measured the responses of two impacts. The results showed that the composite plate with Ni-Ti SMA wires were subjected to a second impact with a peak deflection of 5.47 mm, which was only 0.22 mm larger than the first impact. The relevant data of the composite plate without Ni-Ti SMA wires were 9.02 mm, 1.22 mm, and serious damage occurred. It was verified that the Ni-Ti SMA wires improved the impact resistance of the composite plate. After studying the impact tests of variable diameters of SMA wires embedded at the low layer of composite plate, it was shown that as the diameter of SMA wires increased, the impact resistance of composite plates was improved.
Keywords: composite plate, super-elastic shape memory alloy, Ni-Ti SMA wires, impact resistance.

1. INTRODUCTION

The need for improved materials with better strength and lower weight leads to the use of composite materials in the vehicle industry. Generally, composite structures are susceptible to a wide range of damage and defects caused by manufacturing and in-service loads. Several studies were performed for impact of composite structure [1]. There is a need to improve impact damage properties of composite structures so as that the integrity of the structure is not compromised.

One possible way to increase impact damage resistance of composite structure is by embedding SMA wires into composite structures. Shape memory alloy (SMA) as one of the most important smart materials is used widely. Super-elastic SMA has the ability to absorb mechanical energy when the configuration is changed. Many researchers have investigated factors affecting the ability of shape memory alloy to absorb energy [2 – 4]. J. Zurbitu [5 – 7] et. al. used the impact test equipment to analyze the phase transition and the ability of SMA wires to absorb energy under different impact velocities and strains. Ma N. [8] et. al. found the ability of shape memory alloy to absorb energy is closely related to martensite and the transformation of martensite.

Jason Treadway [9] investigated the properties of absorb energy of super-elastic shape memory alloys under different temperatures. G.N. Dayananda [10] investigated the capacity of absorb energy of super-elastic shape memory alloy under different velocities and load numbers of stretch. Many researchers studied the impact resistance of composite plates with SMA wires embedded by impact tests. Silvio [11] studied the improvement of composite laminates impact properties by embedding SMA wires is evaluated and indications for design and manufacturing of SMA composites with high-impact properties. Shen Cl [12] et al used the new designed impact testing plant to obtained the impact protection properties of NiTi SMA wires at different impact conditions, both martensite NiTi wires and superelastic NiTi wires were tested at room temperature. Mi-Sun Rim [13] made low-velocity impact tests of several types of composite plates, including composite plates with embedded SMA/Fe/Al wires and conventional composite plates. Amit Kumar Gupta [14] carried out CAI studies to quantify the improvement in damage mitigation properties of GFRP laminates by decrease in size of delamination. CAI testing gives change in residual compressive load-carrying capacity of GFRP laminates after impact.

Recently, many researchers investigated numerically the influence of the integration of thin super-elastic shape memory alloy wires to suppress propagating damage of composite structures. Eun-Ho Kim [15] used the analysis model for SMA thin film which based on Lagoudas' model to investigate the effects of shape memory alloy thin films embedded in composite plates for improving damage resistance of composite structures under low velocity impact. H.K. Cho [16] introduces a non-linear finite element analysis approach to the procedure of modeling hybrid laminate composite shells with embedded shape memory alloy (SMA) wire subjected to coupled structural and thermal loading. M. Shariyat [17] revealed that the impact-induced temperature-rise and temperature-dependency of the material properties increase the start and finish stresses

* Corresponding author. Tel.: +86-18855527215; fax: 0431-85682227.
E-mail address: *gaozh@jlu.edu.cn* (Z. Gao)

of the direct and converse phase transformation mechanisms and lead to larger hysteresis loops, strains, and stresses in the SMA wires. M. Shariyat [18] studied the effects of the strain-rate dependency of the elastic moduli of the composite and shape memory alloy (SMA) materials on responses of rectangular composite plates with embedded SMA wires subjected to impacts with spherical indenters. S.M.R. Khalili [19] used the one-dimensional thermodynamic constitutive model by Liang and Rogers to estimate the structural recovery stress. The two-degrees-of-freedom springs-masses model is used to evaluate the contact force between the curved composite plate and the impactor. M. Shariyat [20] presented a higher-order global-local hyperbolic plate theory that includes both odd and even functions. Consequently, is especially adequate for description of the general asymmetric displacement fields. M. Meo [21] experimentally and numerically investigates the response of a smart hybrid thermoplastic composite plate subjected to low-velocity impact. By embedding the SMA wires into the composite plate an increase of the damage resistance is observed with respect to conventional composites structures. Michele Guida [22] carried out Experimental impact tests on both CFRP and hybrid specimens in order to assess the influence of the hybrid fabric on the impact behaviour of structures. The low velocity impact tests have demonstrated the greater energy absorbing capability during the impact of the specimens containing the hybrid layers. In a review [23] of the state of the art of shape memory alloys in hybrid composites for the purpose of damage suppression, the active and passive damage suppression mechanisms are presented.

At present, the impact of composite plate with Ni-Ti SMA wires is mainly confined to simulation studies, such as the use of interface elements and Chang-Chang failure criteria to simulate the damage of composite plate. While the impact test studies of composite plate with Ni-Ti SMA wires are less, the effect of Ni-Ti SMA wires on the impact response of composite plate is lack of experimental verification. In this paper, the experimental verification is carried out to make the research process more systematic and improve the reliability of the conclusion.

2. EXPERIMENTAL DETAILS

2.1. Theoretical basis

2.1.1. The balance of energy under the impact of low velocity

According to the theory of the balance of energy, the kinetic energy (view impactor as rigid object) is translates totally to strain energy and the contact energy of the plate and the energy absorbed by SMA:

$$\frac{1}{2}m_c V_0^2 = U + U_c + U_1, \tag{1}$$

where m_c is weight of impactor, V_0 is velocity of impactor before impact, U is strain energy of composite plate, U_c is contact energy of composite plate, U_1 is energy absorbed by SMA.

2.1.2. The energy absorbed by SMA wire

The superelasticity makes the stress-strain curve of Ni-Ti SMA wire not overlap during a certain degree of loading-unloading process, forming a hysteresis loop and returning to its original state after unloading without residual strain. The dissipated mechanical energy of the Ni-Ti SMA wire is related to the area enclosed by the hysteresis loop. That is, the strain energy absorbed during the loading of the Ni-Ti SMA wire minus the strain energy released during the unloading process has a larger hysteresis loop area. The more mechanical energy dissipated in a circle, the more it will be. When the maximum stress is lower than the initial stress σ_{ms} of martensitic transformation (ie, $\sigma < \sigma_{ms}$), the stress-strain curve overlaps, and there is no hysteresis loop, so the single-loop dissipation energy is zero. When the stress reaches the end of the martensitic transformation stress σ_{mf} (ie, $\sigma_{mf} \leq \sigma$) and then unloaded, the area enclosed by the hysteresis loop is the largest, and the dissipated energy of the single loop reaches the maximum. When $\sigma_{ms} < \sigma < \sigma_{mf}$ is unloaded again, the area of the hysteresis loop is small, and the energy consumption is also small. According to the piecewise linear model in the previous three cases, the energy consumption in the corresponding case can be calculated.

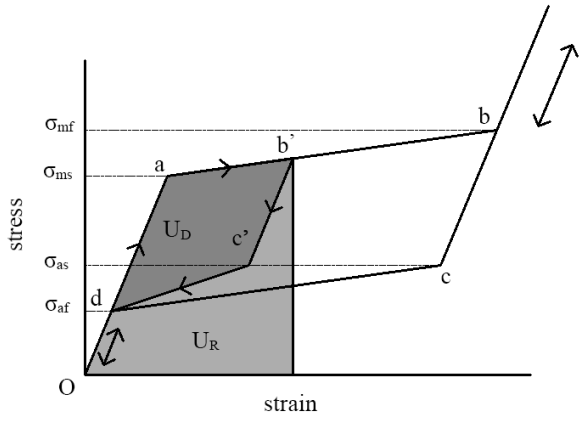

Fig. 1. Strain energy absorbed by SMA

As shown in Fig. 1, the area enclosed by the hysteresis loop ‘ab'c'd’ enclosed by the stress-strain curve of the unloading-unloading process is U_D, i.e. the energy consumed by a lap cycle. When loading stress arrive the end point b, the area of the shadow formed by the hysteresis loop ‘abcd’ is the maximum single-loop energy consumption U_{Dmax}, the unloading line ‘b'c'do’ and the strain axis The shaded area is the strain energy U_R released during unloading. The strain energy absorbed by Ni-Ti SMA wire during loading is:

$$U_A = U_D + U_R. \tag{2}$$

The strain energy U_D dissipated by the single-ring cycle of the Ni-Ti SMA wire is the strain energy U_A absorbed by the load minus the unloaded strain energy UR. In order to obtain the maximum U_{Dmax} of single ring energy consumption, it is necessary to calculate the strain energy of each segment.

The unit volume strain energy absorbed in the ‘oa’ section is:

$$U_{oa} = \int_0^{\varepsilon_a} \sigma d\varepsilon = \int_0^{\varepsilon_a} E_A \varepsilon d\varepsilon = \frac{1}{2}\sigma_{ms}\varepsilon_a, \tag{3}$$

where ε_a is the deformation of point a, σ_{ms} is the stress of point a. E_A is the elastic modulus of section ‘o-a’.

The unit volume strain energy absorbed in the 'ab' section is:

$$U_{\mathrm{ab}} = \int_{\varepsilon_{\mathrm{a}}}^{\varepsilon_{\mathrm{b}}} \sigma \mathrm{d}\varepsilon = \int_{\varepsilon_{\mathrm{a}}}^{\varepsilon_{\mathrm{b}}} (E_{\mathrm{ab}}\,(\varepsilon - \varepsilon_{\mathrm{a}}) + \sigma_{ms})\mathrm{d}\varepsilon = \frac{1}{2}(\sigma_{\mathrm{ms}} + \sigma_{mf})(\varepsilon_b - \varepsilon_{\mathrm{a}}), \quad (4)$$

where ε_{b} is the deformation of point b, σ_{mf} is the stress of point b. E_{ab} is the elastic modulus of section 'a-b'.

The unit volume strain energy released in the bc section is:

$$U_{\mathrm{bc}} = \int_{\varepsilon_{\mathrm{c}}}^{\varepsilon_{\mathrm{b}}} \sigma \mathrm{d}\varepsilon = \int_{\varepsilon_{\mathrm{c}}}^{\varepsilon_{\mathrm{b}}} (E_{\mathrm{M}}(\varepsilon - \varepsilon_{\mathrm{b}}) + \sigma_{\mathrm{mf}})\mathrm{d}\varepsilon = (\varepsilon_b - \varepsilon_{\mathrm{c}})\left[\sigma_{\mathrm{mf}} - \frac{1}{2}E_{\mathrm{M}}(\varepsilon_{\mathrm{b}} - \varepsilon_{\mathrm{c}})\right] = \frac{1}{2}(\sigma_{mf} + \sigma_{\mathrm{as}})(\varepsilon_b - \varepsilon_{\mathrm{c}}), \quad (5)$$

where ε_{c} is the deformation of point c, σ_{as} is the stress of point c. E_M is the elastic modulus of section 'b-c'.

The unit volume strain energy released in the cd section is:

$$U_{cd} = \int_{\varepsilon_{\mathrm{d}}}^{\varepsilon_{\mathrm{c}}} \sigma \mathrm{d}\varepsilon = \int_{\varepsilon_{\mathrm{d}}}^{\varepsilon_{\mathrm{c}}} \left(E_{\mathrm{cd}}(\varepsilon - \varepsilon_{\mathrm{d}}) + \sigma_{sf}\right)\mathrm{d}\varepsilon = (\varepsilon_c - \varepsilon_{\mathrm{d}})\left[\sigma_{as} - \frac{1}{2}E_{cd}(\varepsilon_c - \varepsilon_{\mathrm{d}})\right] = \frac{1}{2}(\sigma_{af} + \sigma_{as})(\varepsilon_c - \varepsilon_{\mathrm{d}}), \quad (6)$$

where ε_{d} is the deformation of point d, σ_{af} is the stress of point d. E_{cd} is the elastic modulus of section 'c-d'.

The unit volume strain energy released in the do section is:

$$U_{do} = \int_0^{\varepsilon_{\mathrm{d}}} \sigma \mathrm{d}\varepsilon = \int_0^{\varepsilon_{\mathrm{d}}} E_A \varepsilon \mathrm{d}\varepsilon = \frac{1}{2}E_A\varepsilon_{\mathrm{d}}^2 = \frac{1}{2}\sigma_{af}\varepsilon_{\mathrm{d}}. \quad (7)$$

According to the Eq. 2 – Eq. 7 for strain energy per unit volume, the maximum strain energy per unit volume of Ni-Ti SMA wire dissipated in a single-cycle cycle can be obtained as:

$$U_{Dmax} = U_{\mathrm{oa}} + U_{\mathrm{ab}} - U_{bc} - U_{cd} - U_{do} = \frac{1}{2}\sigma_{\mathrm{ms}}\varepsilon_{\mathrm{b}} + \frac{1}{2}\sigma_{\mathrm{mf}}(\sigma_c - \sigma_{\mathrm{a}}) - \frac{1}{2}\sigma_{as}(\varepsilon_b - \varepsilon_{\mathrm{d}}) - \frac{1}{2}\sigma_{af}\varepsilon_c. \quad (8)$$

when $\sigma_{ms} < \sigma < \sigma_{mf}$ is unloaded, that is, the unloading line is b'c'do, the area U_D of the hysteresis loop 'ab'c'd' enclosed by it is within abcd:

$$U_D = U_{\mathrm{oa}} + U_{\mathrm{ab'}} - U_{\mathrm{c'b'}} - U_{\mathrm{dc'}} - U_{\mathrm{od}} = \int_0^{\varepsilon_{\mathrm{a}}} E_A \varepsilon \mathrm{d}\varepsilon + \int_{\varepsilon_{\mathrm{a}}}^{\varepsilon_{\mathrm{b'}}} (E_{\mathrm{ab}}\,(\varepsilon - \varepsilon_{\mathrm{a}}) + \sigma_{\mathrm{ms}})\mathrm{d}\varepsilon - \int_{\varepsilon_{\mathrm{c'}}}^{\varepsilon_{\mathrm{b'}}} (E_{b'c'}(\varepsilon - \varepsilon_{\mathrm{b'}}) + E_{\mathrm{ab}}(\varepsilon_{\mathrm{b'}} - \varepsilon_{\mathrm{a}}) + \sigma_{\mathrm{ms}})\mathrm{d}\varepsilon - \int_{\varepsilon_{\mathrm{d}}}^{\varepsilon_{\mathrm{c'}}} (\mathrm{E_{c'd}}(\varepsilon - \varepsilon_{\mathrm{c}}) + \sigma_{\mathrm{as}})\mathrm{d}\varepsilon - \int_0^{\varepsilon_{\mathrm{d}}} \mathrm{E_A}\varepsilon \mathrm{d}\varepsilon\,. \quad (9)$$

2.1.3. Energy absorption equation of superelastic Ni-Ti SMA wires

The energy absorption of the superelastic Ni-Ti SMA is the area enclosed by the stress-strain curve and the strain axis. The yield stress of the superelastic Ni-Ti SMA wire can reach 1 % – 2 %, and the yield stress is about 600 MPa, which is higher than that of ordinary metal. Therefore, the stress level of the loaded stress-strain plateau is higher. And its maximum resilience is up to 8 %, so super-elastic Ni-Ti alloy has excellent energy absorption characteristics, can absorb a lot of strain energy in the loading process, and has no residual strain after unloading.

(1) When $\sigma < \sigma_{\mathrm{ms}}$, $0 < \varepsilon' < \varepsilon_{\mathrm{a}}$, the strain energy absorbed by Ni-Ti SMA wire is:

$$U_{\mathrm{A}} = \int_0^{\varepsilon'} \sigma \mathrm{d}\varepsilon = \int_0^{\varepsilon'} E_{\mathrm{A}}\varepsilon \mathrm{d}\varepsilon = \frac{1}{2}E_{\mathrm{A}}\varepsilon'^2. \quad (10)$$

(2) When $\sigma_{\mathrm{ms}} \le \sigma \le \sigma_{\mathrm{mf}}$, $\varepsilon_{\mathrm{a}} \le \varepsilon' \le \varepsilon_{\mathrm{b}}$, the strain energy absorbed by Ni-Ti SMA wire is:

$$U_A = \int_0^{\varepsilon'} \sigma \mathrm{d}\varepsilon = \int_0^{\varepsilon_{\mathrm{a}}} \mathrm{E_A}\varepsilon \mathrm{d}\varepsilon + \int_{\varepsilon_{\mathrm{a}}}^{\varepsilon'} (\mathrm{E_{ab}}(\varepsilon - \varepsilon_{\mathrm{a}}) + \sigma_{\mathrm{ms}})\mathrm{d}\varepsilon = \frac{1}{2}\sigma_{\mathrm{ms}}\varepsilon_{\mathrm{a}} + \frac{1}{2}\frac{\sigma_{\mathrm{mf}} - \sigma_{\mathrm{ms}}}{\varepsilon_{\mathrm{b}} - \varepsilon_{\mathrm{a}}}(\varepsilon' - \varepsilon_{\mathrm{a}})^2 + \sigma_{\mathrm{ms}}(\varepsilon' - \varepsilon_{\mathrm{a}}).$$

(3) When $\sigma_{\mathrm{mf}} < \sigma$, $\varepsilon_{\mathrm{b}} < \varepsilon'$, the strain energy absorbed by Ni-Ti SMA wire is:

$$U_A = \int_0^{\varepsilon'} \sigma \mathrm{d}\varepsilon = \int_0^{\varepsilon_{\mathrm{a}}} \mathrm{E_A}\varepsilon \mathrm{d}\varepsilon + \int_{\varepsilon_{\mathrm{a}}}^{\varepsilon_{\mathrm{b}}} (\mathrm{E_{ab}}(\varepsilon - \varepsilon_{\mathrm{a}}) + \sigma_{\mathrm{ms}})\mathrm{d}\varepsilon + \int_{\varepsilon_{\mathrm{b}}}^{\varepsilon'} (\mathrm{E_M}(\varepsilon - \varepsilon_{\mathrm{b}}) + \sigma_{\mathrm{mf}})\mathrm{d}\varepsilon = \frac{1}{2}\sigma_{\mathrm{ms}}\varepsilon_{\mathrm{a}} + \frac{1}{2}(\sigma_{\mathrm{ms}} + \sigma_{\mathrm{mf}})(\varepsilon_{\mathrm{b}} - \varepsilon_{\mathrm{a}}) + \frac{1}{2}\mathrm{E_M}\ (\varepsilon' - \varepsilon_{\mathrm{b}})^{\ 2} + \sigma_{\mathrm{mf}}(\varepsilon' - \varepsilon_{\mathrm{b}})\,.$$

2.2. Low-velocity impact tests at the SMA composite

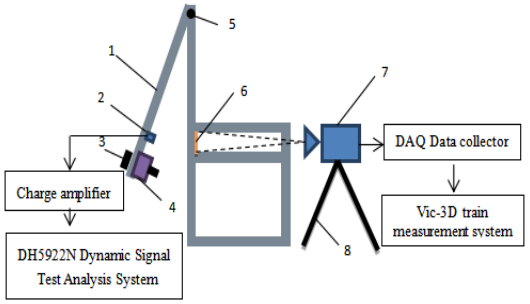

Fig. 2. Composite plate impact test schematic

Fig. 2 is a schematic of a composite plate impact test device. The composite plate is fixed on a support table. In order to facilitate the collection of the response of the plane strain, center deflection, etc. During the impact process, a pendulum hammer horizontal impact composite plate design method was adopted. The impact energy consists of two parts, one is the impact energy of the gravity potential energy of the mass into the falling process, and the other is the impact energy of the pendulum's own gravity potential energy during the falling process. The mass is installed on the lower end of the pendulum, setting its mass to m_1, drop height h, then the impact energy of the mass's gravitational potential energy is converted into $Q_1 = m_1 gh$; the center of mass of the pendulum is in the center position, and the mass of the pendulum is set, The drop height is $h/2$ for m_2, then the impact energy of the pendulum's gravitational potential energy is $Q_2 = m_2 g\, h/2$, and the impact energy is the sum of Q_1 and Q_2. The force sensor is installed on the lower end of the swing rod. During the impact process, the metal punch at the front end of the force sensor contacts the composite material plate to collect contact force information. The xy plane strain and deflection data of the impact back surface of the composite plate was collected by a Vic-3D-v7 non-contact full-field strain measurement system equipped with two high-speed cameras. The absorption energy of the composite plate is obtained by the formula $\int F_i \times \Delta h_i\, dh$, where F_{i} is the impact force in the ith time period. During this period, F_i can be regarded as a fixed value, generally taking the middle The value, Δh_{i} is

the amount of deflection change during this period of time, and the entire impact process is integrated to obtain the energy absorption curve of the composite plate during the impact process.

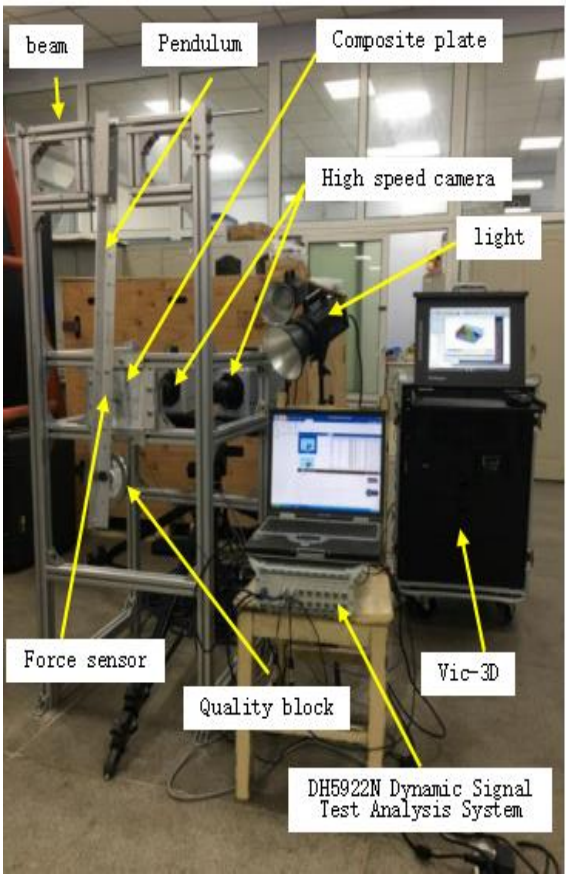

Fig. 3. Composite plate impact test bench

2.3. Glass fiber composite contact forming for composite plate

Contact molding is to apply mold release agent on the polished mold first, and then lay reinforcement materials such as glass fiber cloth and glass blanket on the mold, brush the prepared epoxy resin matrix on the glass fiber cloth with tools such as brush, repeat the above operations until the layer reaches the required thickness of the sample, and demould after curing at room temperature or heating, without pressure or low pressure.

In this experiment, 191 type epoxy resin with good fluidity and low viscosity was selected to facilitate brush coating and reduce bubbles generated during stirring.

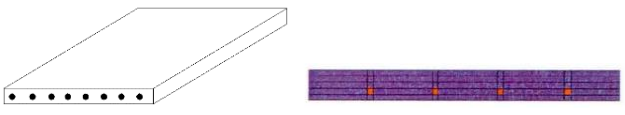

a b

Fig. 4. Composite plate schematic: a – sketch map; b – specific laying position of SMA wire

In the experiment, the glass fiber cloth woven with super elastic NiTi SMA wire is used as the fourth layer, as shown in Fig. 4 b. The composite plate with the size of 170 mm × 170 mm is prepared, in which the width of 10 mm is reserved on each side as the clamping part, so the effective size is 150 mm × 150 mm.

There are five layers of composite material plate with thickness of 2 mm. The number of NiTi SMA wires in composite plates is 50, and the spacing is 3 mm. The specific parameters of alloy wires are shown in Table 1. The impact tests of composite plates with and without hyperelastic NiTi SMA wires were carried out by using the impact test device in Section 2.2. When the mass of the mass block is 2 kg and the pendulum is 0.8 kg, the falling height of the mass block is 375 mm. The impact energy is obtained from the gravitational potential energy of the mass block and the pendulum, and the impact energy is 9j.

Table. 1. Ni-Ti SMA wires

Ni-Ti SMA wires	diameter	length
Super-elasticity	0.4 mm	150 mm

3. RESULT AND DISCUSSION

3.1. Comparison of impact responses of composite plates impacted by two impacts

In order to prove the impact on the impact resistance of the composite plate before and after adding the Ni-Ti SMA wires, two composite plants were subjected to two impacts in this section. This paper investigates the changes in the impact resistance of two kinds of composite materials.

Fig. 5 shows the example of the impact response cloud of composite plates. Fig. 6 shows the impact of two impacts on composite plates containing Ni-Ti SMA wires and without Ni-Ti SMA wires.

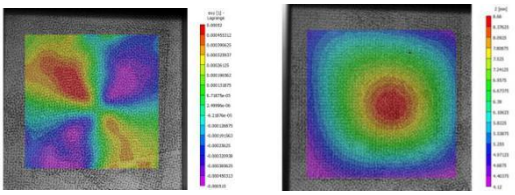

a b

Fig. 5. Impact response cloud of composite plates (example): a – xy plane strain cloud; b – deflection cloud

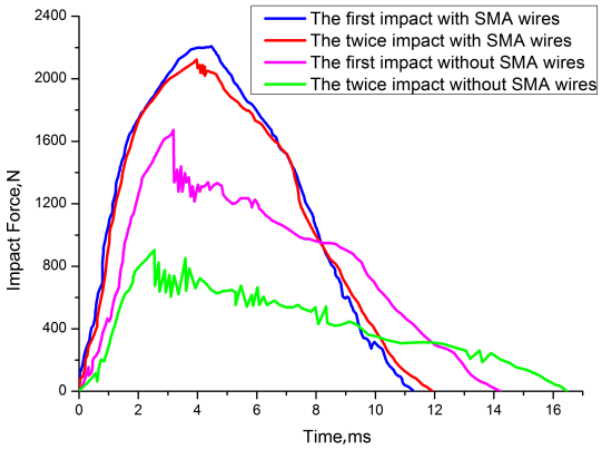

Fig. 6. Impact forces of composite plates impacted by two times

The maximun impact force of the first impact with SMA wires was 2207.12 N, and without SMA wires

maximum was 1672.90 N. The maximun impact force of the twice impact with SMA wires was 2122.51 N, but without SMA wires maximum was 903.79 N. It can be seen from Fig. 6 that the time of the maximum impact force of second impact of the two composite plates advances, which is related to the increase of the energy absorption rate of the two composite plates during the second impact. Fig. 7 shows the deformation of SMA wire plate and non SMA wire plate after the first and second impact. The experimental results show that the maximum deformation of SMA wire plate is 5.26 mm and 5.44 mm respectively during the impact test, but the deformation is reduced to 0 due to the hyperelasticity of SMA wire, and the maximum deformation of 7.89 mm and 9.02 mm for non SMA wire plate, after impact there still have obvious residual deformation.

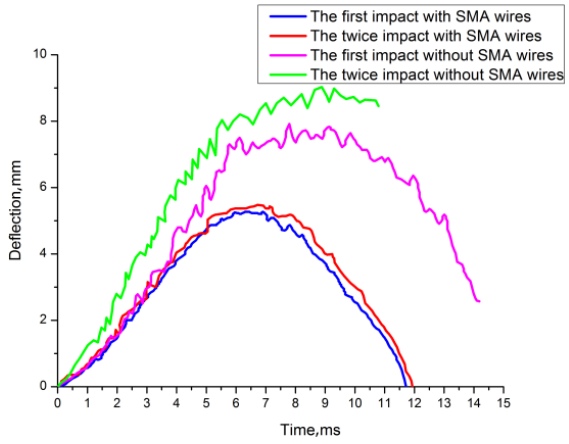

Fig. 7. Deflection of composite plates impacted by two times

It can be seen from the energy absorption curve in Fig. 8 that the residual energy absorption of the composite plate with SMA wire after twice impacts is almost the same, which also shows that the second impact did not cause serious damage to the composite plate. For the material plate without SMA wires, the residual data can not be collected after the twice impact due to the damage at the back of the plate surface.

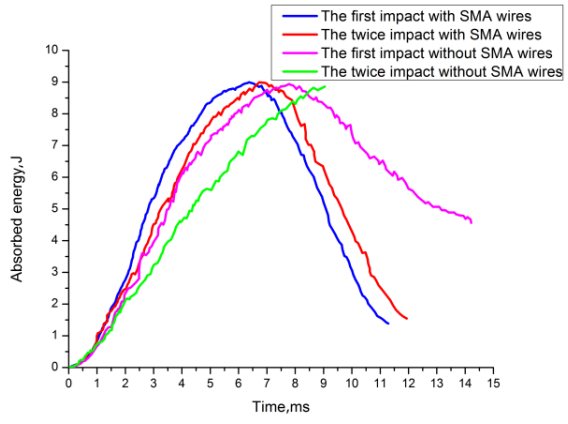

Fig. 8. Absorbed energy of composite plates impacted by two times

It can be seen from the impact peak values of the two impacts of the two composite plates shown in Fig. 9 a that although the peak impact force of the second time has decreased, the impact peak value of the composite plate containing Ni-Ti SMA wire decreases.

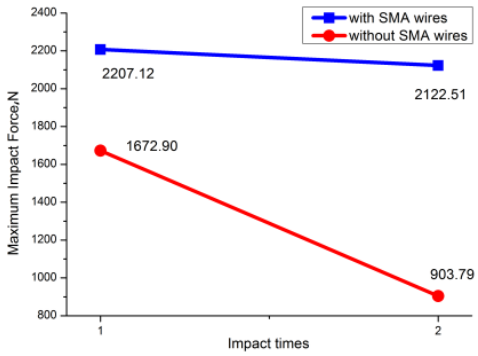

a

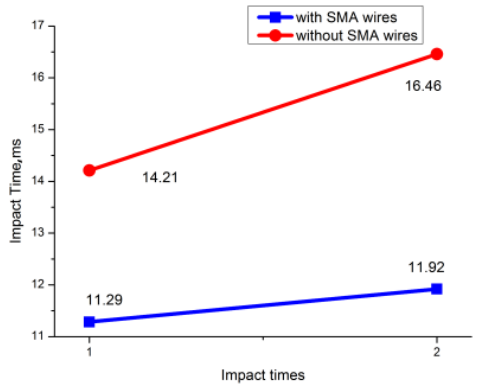

b

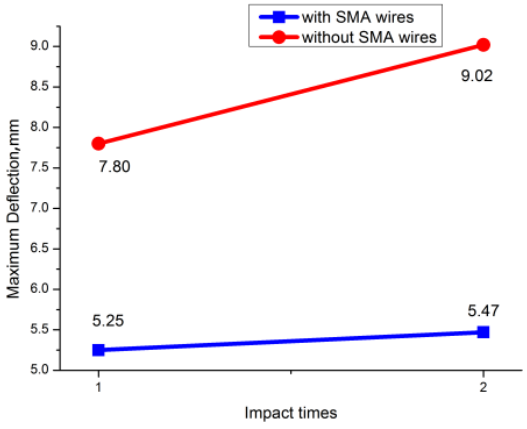

c

Fig. 9. Comparison of two impact responses of composite plates

The amplitude is very small, from 2207.12 N to 2122.51 N, falling by about 3.83 %, and the peak impact force of composite plates without alloy filaments has fallen by a large margin, from 1672.90 N to 903.79 N, falling by about 45.97 %. The two impact force curves of the composite plate with Ni-Ti SMA wires have a good coincidence degree, and the impact force level does not show a significant decrease, indicating that the composite material plate has no large-area damage and has strong ability to withstand impact loads. Combining the deflection curves of the two impacts of the two composite plates of Fig. 10 and the maximum deflection of Fig. 9 b, it can be

seen that the deflection of the second impact of the two composite plates decreases.

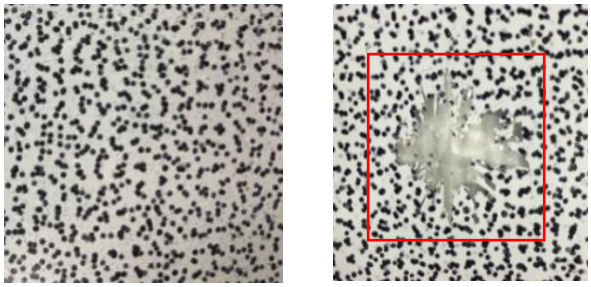

a b

Fig. 10. The effect of composite plates after the second impact: a – with SMA wires; b – without SMA wires

The maximum deflection of the second impact of the composite plate without SMA wires is 9.02 mm, which is 1.22 mm higher than the first impact, and the deflection curve of the second impact has no data after the peak. This is Due to the serious impact damage on the back of the board (Fig. 10 b), there is no speckle on the surface and no data can be collected. The absolute value of the deflection peak of the composite plate incorporating Ni-Ti SMA wires was 5.47 mm, an increase of 0.22 mm with little change. As shown in Fig. 10 a, the secondary impact surface of the composite plate with Ni-Ti SMA wires shows no obvious damage. From the energy absorption curve of Fig. 11, it can be seen that the residual energy absorbed by the composite plate with Ni-Ti SMA wires after two impacts is not much different, which can also indicate that the second impact did not bring the composite plate with serious damage.

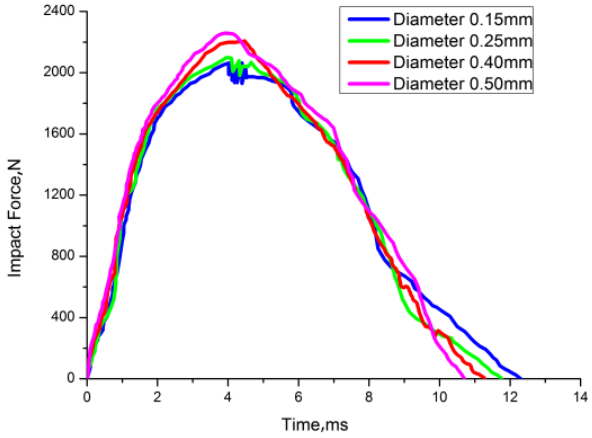

Fig. 11. Impact forces of composite plates with different diameter SMA wires

3.2. Influence of different diameter Ni-Ti SMA wires on impact response of composite plates

Selective Ni-Ti SMA wires with diameters of 0.15 mm, 0.25 mm, 0.40 mm, and 0.50 mm were used as reinforcement fibers to test the impact response of composite plates. The preparation method of the composite material plate, the distribution of the filaments, and the fixing method are the same as the previous experiments, and the impact energy is 9 J.

Fig. 11 is the impact force curve of a composite plate with four different diameters of Ni-Ti SMA wires. It can be seen from the figure that as the diameter of the Ni-Ti SMA wire increases, the slope and peak of the curve increase. The trend shows that the increase in the volume fraction of Ni-Ti SMA wire improves the stiffness of the composite plate and its ability to withstand impact forces. The peak point, the unloading start point, and the end time of the impact have all been advanced. This, along with the increase in the volume fraction of Ni-Ti SMA, also increases the phase transition and lattice shear and consumes more impact energy. Fig. 12 shows the center-deflection curves of a composite plate containing Ni-Ti SMA wires of different diameters.

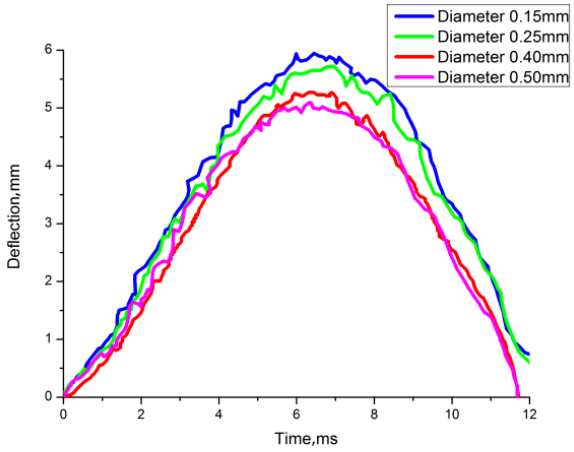

Fig. 12. Deflection of composite plates with different diameter SMA wires

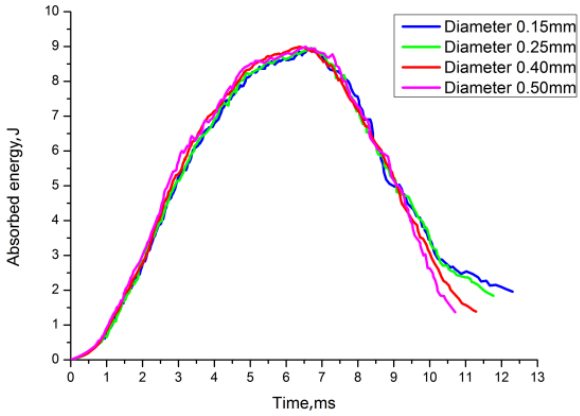

Fig. 13. Absorbed energy of composite plates with different diameter SMA wire

It can be seen from the figure that as the volume content of Ni-Ti SMA increases, the maximum of the deflection of the composite plate decreases and the deflection returns to the starting point, the remaining deflection is reduced. And Fig. 13 shows that as the diameter of Ni-Ti SMA wires increases, the energy absorbed by the composite plate decreases after the impact. In order to visually see the variation of the impact response with the volume content of Ni-Ti SMA, a comparison of the impact responses of composite plates with different diameters of Ni-Ti SMA wires is given in Fig. 14. Where Fig. 14 a is the peak impact force; Fig. 14 b is the maximum deflection; Fig. 14 c is the impact time; Fig. 14 d is the residual deflection; Fig. 14 e is the remaining energy absorbed by the composite plate.

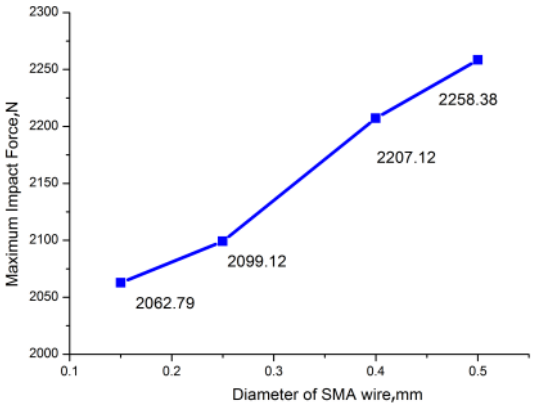

a

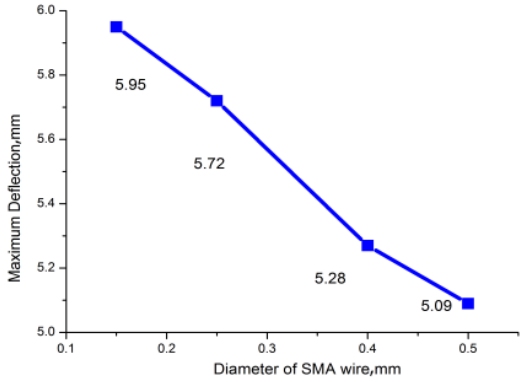

b

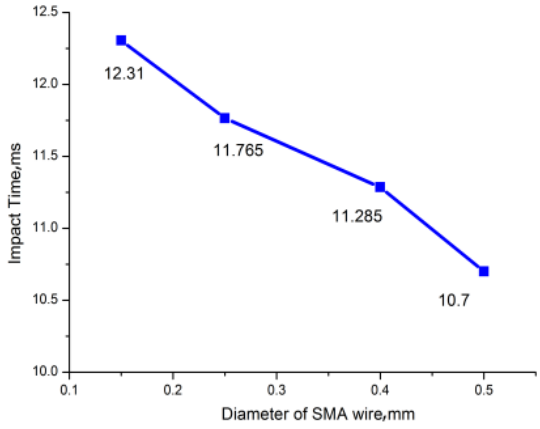

c

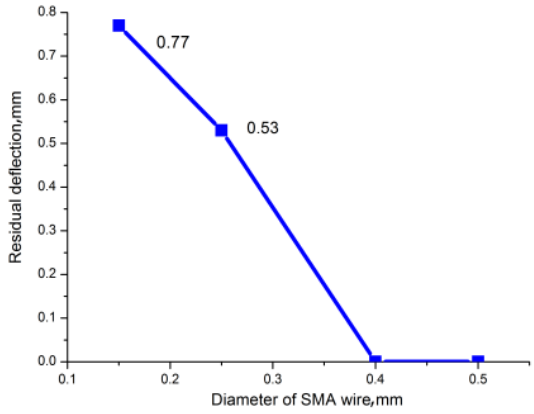

d

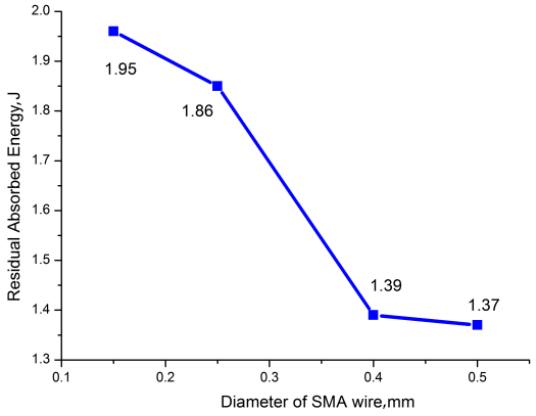

e

Fig. 14. Comparison of impact responses of composite plates with different diameter SMA wires

From the line chart, it can be seen that the peak impact force increases almost linearly with the increase of the diameter of the alloy wire. When the diameter is 0.25 mm to 0.4 mm, the peak impact force growth rate is the fastest. When the diameter is 0.5 mm, the impact force peak value is 2258.38 N. Compared with the peak value of 2062.79 N when the diameter is 0.15 mm, the increase is 9.48 %. From Fig. 14 b and c, it can be seen that the peak deflection and impact time are approximately linear with the diameter of the alloy wire, and decrease as the diameter of the alloy wire increases. It shows that the larger the diameter of the alloy wire, the more impact energy the Ni-Ti SMA wire takes up in absorbing and consuming, so that the impact process ends prematurely and the energy borne by the glass fiber and the matrix is reduced. From Fig. 14 d, it can be seen that the change law of the residual deflection is the same as the conclusion obtained in Fig. 14 b and c. As the impact energy borne by the matrix and the glass fiber is reduced, the energy that causes damage is also reduced. However, it can be seen from the figure that when the diameter reaches 0.4 mm, the residual deflection does not change with the diameter, which means that the elastic deformation, phase change, etc. of the Ni-Ti SMA wires absorb part of the impact energy, and the glass fiber and the resin matrix absorb the energy does not produce significant damage, and there is an excess of Ni-Ti SMA wires' ability to absorb energy. From Fig. 14 e, it can be seen that the remaining energy absorbed by the composite plate decreases with the increase in the diameter of the Ni-Ti SMA wires, and the increase in the diameter from 0.25 mm to 0.40 mm shows the most significant reduction in the remaining energy absorption, which is approximately the same 25.27 % indicates that the Ni-Ti SMA wires significantly inhibited the impact damage of the composite plate, allowing the composite plate to rebound quickly after impact and returning more impact energy to the punch. However, after the diameter increased from 0.40 mm to 0.50 mm, there was no significant change in the remaining energy absorbed, indicating an excess of Ni-Ti SMA wires absorbing ability.

3. CONCLUSIONS

Experiments were conducted on the composite material plate which effective size is 150 mm × 150 mm.

There are five layers of composite material plate with thickness of 2 mm, and Ni-Ti SMA wires laid on the fourth layer. The number of Ni-Ti SMA wires in composite plates is 50, and the spacing is 3 mm. The impact response of the composite plate with Ni-Ti SMA wires and without Ni-Ti SMA wires was 9 J. Studies have shown that:

1. The composite plates with super-elastic Ni-Ti SMA wires can withstand peak impact forces, shorten the impact time, reduce the peak deflection of the impact point, and have a residual deflection of 0. There is basically no visible damage.
2. The decrease of residual energy absorption shows that the composite material plate with the super-elastic Ni-Ti SMA wires has less fiber breakage and less damage to the matrix. The composite material plate can rebound quickly during the impact and return some of the deformation energy to the punch, suppresses the expansion of material damage.
3. Compared with ordinary metal wires, Ni-Ti SMA wires are more effective in improving the ability of composite materials to withstand impact loads. Peak deflection, impact time, and residual deflection are reduced, which reduces impact damage.
4. Comparing with the results of the first impact test, the impact resistance of the composite plate with Ni-Ti SMA wires remains basically unchanged during the second impact, and there is no obvious damage on the back surface. After the second impact of the plate without Ni-Ti SMA wires, significant damage was observed on the back surface, which verified the improved impact resistance of the Ni-Ti SMA wires on the composite material sheet.
5. When the diameter of the Ni-Ti SMA wires exceeds 0.4 mm, the residual deflection of the composite plate is 0, the change of the remaining suction energy is small, the damage degree of the composite plate is small, and the resistance to impact is stable. Therefore, when the laying position and the number of SMA wires are determined, the impact resistance of SMA wires with a diameter of 0.4mm is the best chioce.

Acknowledgments

This project is supported by National Natural Science Foundation of China (Grant No. 51875237), the Science and Technology Development Project of Jilin Province (Project No. 20160101283JC) and the “13th Five-Year” Science and Technology Research Project of Education Department of Jilin Province (Project No. 2016-417).

REFERENCES

1. **Morinière, F.D., Alderliesten, R.C., Sadighi, M., Benedictus, R.** An Integrated Study on the Low-Velocity Impact Response of the GLARE Fibre-Metal Laminate *Composite Structures* 100 2013: pp. 89 – 103. https://doi.org/10.1016/j.compstruct.2012.12.016
2. **Treadway, J., Abolmaali, A., Lu, F., Aswath, P.** Tensile and Fatigue Behavior of Superelastic Shape Memory Rods *Materials and Design* 86 2015: pp. 105 – 113. https://doi.org/10.1016/j.matdes.2015.07.024
3. **Dayananda, G.N., Rao, M.S.** Effect of Strain Rate on Properties of Superelastic NiTi Thin Wires *Materials Science and Engineering A* 486 (1 – 2) 2008: pp. 96 – 103. https://doi.org/10.1016/j.msea.2007.09.006
4. **Saikrishna, C.N., Ramaiah, K.V., Bhagyaraj, J., Gouthama, Bhaumik, S.K.** Influence of Stored Elastic Strain Energy on Fatigue Behaviour of NiTi Shape Memory Alloy Thermal Actuator Wire *Materials Science and Engineering A* 587 2013: pp. 65 – 71. https://doi.org/10.1016/j.msea.2013.08.048
5. **Zurbitu, J., Kustov, S., Castillo, G., Aretxabaleta, L., Cesari, E., Aurrekoetxea, J.** Instrumented Tensile-Impact Test Method for Shape Memory Alloy Wires *Materials Science and Engineering A* 524 (1 – 2) 2009: pp. 108 – 111. https://doi.org/10.1016/j.msea.2009.06.012
6. **Zurbitu, J., Castillo, G., Urrutibeascoa, I., Aurrekoetxea, J.** Low-Energy Tensile-Impact Behavior of Superelastic NiTi Shape Memory Alloy Wires *Mechanics of Materials* 41 (9) 2009: pp. 1050 – 1058. https://doi.org/10.1016/j.mechmat.2009.06.003
7. **Zurbitu, J., Castillo, G., Urrutibeascoa, I., Aurrekoetxea, J.** Effect of Impact-Induced Strain on the Stress-Induced Martensitic Transformation of Superelastic NiTi Shape-Memory Alloy Wires *Journal of Materials Engineering and Performance* 18 (5 – 6) 2009: pp. 600 – 602. https://doi.org/10.1007/s11665-009-9401-2
8. **Ma, N., Song, G.** Study of Damping Capacities of Nitinol Shape-Memory Alloys in Martensite, Austenite, and Martensite-Austenite Co-Existence Phases *Smart Structures and Materials: Damping and Isolation* 2005: pp. 142 – 151. https://doi.org/10.1117/12.604479
9. **Treadway, J., Abolmaali, A., Lu, F., Aswath, P.** Tensile and Fatigue Behavior of Superelastic Shape Memory Rods *Materials and Design* 86 2015: pp. 105 – 113. https://doi.org/10.1016/j.matdes.2015.07.024
10. **Dayananda, G.N., Rao, M.S.** Effect of Strain Rate on Properties of Superelastic NiTi Thin Wires *Materials Science and Engineering A* 486 (1 – 2) 2008: pp. 96 – 103. https://doi.org/10.1016/j.msea.2007.09.006
11. **Pappadà, S., Rametta, R., Toia, L., Coda, A., Fumagalli, L., Maffezzoli, A.** Embedding of Superelastic SMA Wires into Composite Structures: Evaluation of Impact Properties *Journal of Materials Engineering and Performance* 18 (5 – 6) 2009: pp. 522 – 530. https://doi.org/10.1007/s11665-009-9366-1
12. **Shen, C., Wu, Z., Gao, Z., Ma, X., Qiu, S., Liu, Y., Sun, T.** Impact Protection Behavior of NiTi Shape Memory Alloy Wires *Materials Science and Engineering A* 700 2017: pp. 132 – 139. http://dx.doi.org/10.1016/j.msea.2017.05.097
13. **Rim, M.S., Kim, E.H., Lee, I., Choi, I.H., Ahn, S.M., Koo, K.N., Bae, J.S., Roh, J.H.** Low-Velocity Impact Characteristics of Composite Plates with Shape Memory Alloy Wires *Journal of Theoretical and Applied Mechanics* 49 (3) 2011: pp. 841 – 857. http://orcid.org/0000-0002-9842-2468
14. **Gupta, A.K., Velmurugan, R., Joshi, M., Gupta, N.K.** Studies on Shape Memory Alloy-Embedded GFRP Composites for Improved Post-Impact Damage Strength *International Journal of Crashworthiness* 2018: pp. 1 – 17. https://doi.org/10.1080/13588265.2018.1452549
15. **Kim, E.H., Lee, I., Roh, J.H., Bae, J.S., Choi, I.H., Koo, K.N.** Effects of Shape Memory Alloys on Low Velocity Impact Characteristics of Composite Plate *Composite Structures* 93 (11) 2011: pp. 2903 – 2909.

https://doi.org/10.1016/j.compstruct.2011.05.013

16. **Cho, H.K., Rhee, J.** Nonlinear Finite Element Analysis of Shape Memory Alloy (SMA) Wire Reinforced Hybrid Laminate Composite Shells *International Journal of Non–Linear Mechanics* 47 (6) 2012: pp. 672 – 678. https://doi.org/10.1016/j.ijnonlinmec.2011.11.002
17. **Shariyat, M., Niknami, A.** Layerwise Numerical and Experimental Impact Analysis of Temperature-Dependent Transversely Flexible Composite Plates with Embedded SMA Wires in Thermal Environments *Composite Structures* 153 2016: pp. 692 – 703. https://doi.org/10.1016/j.compstruct.2016.06.070
18. **Shariyat, M., Niknami, A.** Impact Analysis of Strain-Rate-Dependent Composite Plates with SMA Wires in Thermal Environments: Proposing Refined Coupled Thermoelasticity, Constitutive, and Contact Models *Composite Structures* 136 2016: pp. 191 – 203. https://doi.org/10.1016/j.compstruct.2015.10.003
19. **Khalili, S.M.R., Ardali, A.** Low-Velocity Impact Response of Doubly Curved Symmetric Cross-Ply Laminated Panel with Embedded SMA Wires *Composite Structures* 105 2013: pp. 216 – 226. https://doi.org/10.1016/j.compstruct.2013.04.041
20. **Shariyat, M., Hosseini, S.H.** Accurate Eccentric Impact Analysis of the Preloaded SMA Composite Plates, Based on a Novel Mixed-Order Hyperbolic Global–Local Theory *Composite Structures* 124 2015: pp. 140 – 151. https://doi.org/10.1016/j.compstruct.2015.01.002
21. **Meo, M., Marulo, F., Guida, M., Russo, S.** Shape Memory Alloy Hybrid Composites for Improved Impact Properties for Aeronautical Applications *Composite Structures* 95 2013: pp. 756 – 766. https://doi.org/10.1016/j.compstruct.2012.08.011
22. **Guida, M., Sellitto, A., Marulo, F., Riccio, A.** Analysis of the Impact Dynamics of Shape Memory Alloy Hybrid Composites for Advanced Applications *Materials* 12 (1) 2019: pp. 153. https://doi.org/10.3390/ma12010153
23. **Angioni, S.L., Meo, M., Foreman, A.** Impact Damage Resistance and Damage Suppression Properties of Shape Memory Alloys in Hybrid Composites–a Review *Smart Materials and Structures* 20 (1) 2010: pp. 013001. https://doi.org/10.1088/0964-1726/20/1/013001